Mineralogical Magazine (2019), **83**, 115–121
doi:10.1180/mgm.2018.112

CAMBRIDGE UNIVERSITY PRESS

Article

Ammoniomathesiusite, a new uranyl sulfate–vanadate mineral from the Burro mine, San Miguel County, Colorado, USA

Anthony R. Kampf[1], Jakub Plášil[2], Barbara P. Nash[3] and Joe Marty[4]

[1]Mineral Sciences Department, Natural History Museum of Los Angeles County, 900 Exposition Boulevard, Los Angeles, CA 90007, USA; [2]Institute of Physics ASCR, v.v.i., Na Slovance 1999/2, 18221 Prague 8, Czech Republic; [3]Department of Geology and Geophysics, University of Utah, Salt Lake City, Utah 84112, USA; and [4]5199 East Silver Oak Road, Salt Lake City, UT 84108, USA

Abstract

The new mineral ammoniomathesiusite $(NH_4)_5(UO_2)_4(SO_4)_4(VO_5)\cdot 4H_2O$, was found in the Burro mine, San Miguel County, Utah, USA, where it occurs as a secondary phase on asphaltum/quartz matrix in association with ammoniozippeite, gypsum, jarosite and natrozippeite. The mineral forms pale yellow to greenish-yellow prisms, up to ~0.3 mm long, with pale-yellow streak and bright yellow–green fluorescence. Crystals are transparent and have vitreous lustre. The mineral is brittle, with Mohs hardness of 2½, stepped fracture and two cleavages: excellent on {110} and good on {001}. The calculated density is 3.672 g/cm^3. Ammoniomathesiusite is optically uniaxial (–) with $\omega = 1.653(2)$ and $\epsilon = 1.609(2)$ (white light). Pleochroism is: O = green-yellow, E = colourless; $O > E$. Electron microprobe analyses yielded the empirical formula $[(NH_4)_{4.75}(UO_2)_4(SO_4)_4(VO_5)\cdot 4(H_{2.07}O)$. The five strongest powder X-ray diffraction lines are [d_{obs} Å(I)(hkl)]: 10.57(46)(110), 7.10(62)(001), 6.41(100)(101), 3.340(35)(240) and 3.226(44)(141). Ammoniomathesiusite is tetragonal, $P4/n$ with $a = 14.9405(9)$, $c = 7.1020(5)$ Å, $V = 1585.3(2)$ Å^3 and $Z = 2$. The structure of ammoniomathesiusite ($R_1 = 0.0218$ for 3427 $I > 2\sigma I$) contains heteropolyhedral sheets based on $[(UO_2)_4(SO_4)_4(VO_5)]^{5-}$ clusters. The structure is identical to that of mathesiusite, with NH_4^+ in place of K^+.

Keywords: ammoniomathesiusite, new mineral, uranyl sulfate–vanadate, crystal structure, Burro mine, Colorado, USA

(Received 7 January 2018; accepted 26 January 2018)

Introduction

The Uravan Mineral Belt of the Colorado Plateau, which spans the Colorado–Utah border, has been a rich source of uranium and vanadium ores. The mines in this belt have also yielded many new secondary U and V minerals, the first of which was carnotite, $K_2(UO_2)_2(VO_4)_2\cdot 3H_2O$, described from the Rajah mine in the northern portion of the belt by Friedel and Cumenge (1899). Although mining in what is now called the Slick Rock district in the southern portion of the belt dates to around 1900, apparently the Burro mine in that district was not active until the mid-1950s. The first new mineral to be described from the Burro mine was metamunirite, $NaVO_3$ (Evans, 1991), and recently burroite, $Ca_2(NH_4)_2(V_{10}O_{28})\cdot 15H_2O$, was described (Kampf *et al.*, 2017). Herein, we describe ammoniomathesiusite, the third new mineral from the Burro mine.

Ammoniomathesiusite is named as the ammonium analogue of mathesiusite, $K_5(UO_2)_4(SO_4)_4(VO_5)\cdot 4H_2O$ (Plášil *et al.*, 2014), with NH_4^+ in place of K^+. The new mineral and name were approved by the Commission on New Minerals, Nomenclature and Classification of the International Mineralogical Association (IMA2017-077). The holotype and three cotypes are deposited in the collections of the Natural History Museum of Los Angeles County, 900 Exposition Boulevard, Los Angeles, CA 90007, USA, catalogue numbers 67248 (holotype), 67249, 67250 and 69251.

Occurrence

Ammoniomathesiusite was collected underground at the Burro mine, Slick Rock district, San Miguel County, Colorado, USA (38°2'42"N, 108°53'23"W). The Burro mine is near the southern end of the Uravan Mineral Belt, in which uranium and vanadium minerals occur together in bedded or roll-front deposits in the sandstone of the Salt Wash member of the Jurassic Morrison Formation (Carter and Gualtieri, 1965; Shawe, 2011). The uranium and vanadium ore mineralisation was deposited where solutions rich in U and V encountered pockets of strongly reducing solutions that had developed around accumulations of carbonaceous plant material, still in evidence as carbonised plant remains and notable logs. Mining operations have exposed both unoxidised and oxidised U and V phases. Under ambient temperatures and generally oxidising near-surface conditions, water reacts with pyrite and chalcopyrite to form aqueous solutions with relatively low pH, which then react with the earlier-formed montroseite–corvusite assemblages, resulting in diverse suites of secondary minerals. The NH_4^+ presumably derives from organic matter in the deposit.

Ammoniomathesiusite is rare and occurs on asphaltum/quartz matrix in association with ammoniozippeite (Kampf *et al.*, 2018),

Author for correspondence: Anthony R. Kampf, Email: akampf@nhm.org
Associate Editor: Juraj Majzlan
Cite this article: Kampf A.R., Plášil, J., Nash B.P. and Marty J. (2019) Ammoniomathesiusite, a new uranyl sulfate–vanadate mineral from the Burro mine, San Miguel County, Colorado, USA. *Mineralogical Magazine*, **83**, 115–121. https://doi.org/10.1180/mgm.2018.112

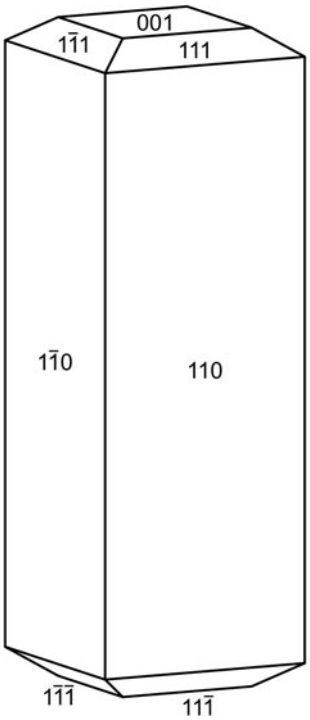

Fig. 1. Crystal drawing of ammoniomathesiusite crystal; clinographic projection.

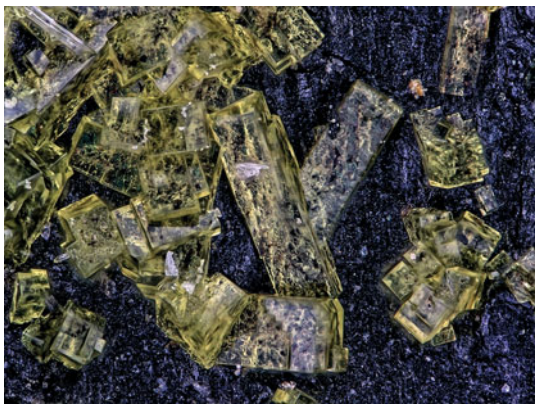

Fig. 2. Ammoniomathesiusite prisms on asphaltum. The field of view is 0.84 mm across.

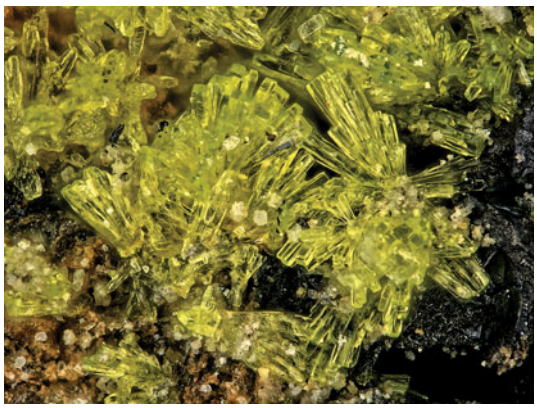

Fig. 3. Sprays of ammoniomathesiusite prisms on asphaltum. The field of view is 0.84 mm across.

gypsum, jarosite and natrozippeite. Other secondary minerals verified by us to occur in the mine include: andersonite, ansermetite, barnesite, brochantite, burroite (Kampf *et al.*, 2017), calciodelrioite, calcite, chalcomenite, grantsite, gunterite, hewettite, huemulite, hughesite, hydrocerussite, kokinosite, lasalite, lindgrenite, magnesiopascoite, martyite, metamunirite, metarossite, metaschoepite, munirite, navajoite, orthoserpierite, pascoite, rossite, schindlerite, schröckingerite, serpierite, sherwoodite, strelkinite, tyuyamunite, uranopilite, volborthite, wernerbaurite, zippeite and numerous other potentially new minerals, currently under study.

Physical and optical properties

Ammoniomathesiusite crystals are {110} prisms, up to ~0.3 mm long, with square cross-sections and flat {001} terminations, sometimes modified by {111} pyramids (Fig. 1). Broad prisms are typically isolated or intergrown in random orientations (Fig. 2); narrow prisms, often tapering slightly towards their terminations, occur in sprays or bow-tie-like intergrowths (Fig. 3). No twinning was observed.

Crystals are yellow to greenish yellow and transparent with vitreous lustre. The streak is very pale yellow. The mineral fluoresces bright yellow–green under a 405 nm laser. The Mohs hardness is 2½, based upon scratch tests. Crystals are brittle with stepped fracture and two cleavages: excellent on {110} and good on {001}. At room temperature, the mineral decomposes in H_2O. The density could not be measured because the mineral decomposes in Clerici solution. The calculated density based on the empirical formula is 3.672 g/cm^3. Optically, ammoniomathesiusite is uniaxial (–), with $\omega = 1.653(2)$ and $\epsilon = 1.609(2)$, measured in white light. The mineral is distinctly pleochroic: O = green yellow, E colourless; $O > E$.

Raman spectroscopy

Raman spectroscopy was conducted on a Horiba XploRA PLUS spectrometer. Pronounced fluorescence was observed using a 532 nm diode laser; consequently, a 785 nm diode laser was utilised. The power density of the laser beam at the sample was 9.6 mW. The spectrum was recorded from 2000 to 100 cm^{-1}, but was featureless between 2000 and 1200 cm^{-1}. The spectrum from 1400 to 100 cm^{-1}, is shown in Fig. 4.

The broad band of low intensity at ~1200 cm^{-1} is probably an overtone or combination band; a band at nearly the same frequency was observed in the spectrum of mathesiusite (Plášil *et al.*, 2014), however, with an incorrect assignment. Very weak Raman bands at 1110 cm^{-1} and at 1090 cm^{-1} and a broader band at 1057 cm^{-1} with a shoulder at 1065 cm^{-1} are attributed to split triply degenerate ν_3 antisymmetric stretching vibrations of the SO_4 tetrahedron. A sharp, slightly asymmetric two-component band of medium intensity at 1010 cm^{-1} is assigned to the ν_1 symmetric stretching vibration of the SO_4 tetrahedron. A sharp band at 977 cm^{-1} is attributed to the symmetric ν_1 (V–O) stretching mode (*cf.* Plášil *et al.*, 2014; Frost *et al.*, 2005). A weak two-component overlapping band at 904 and 894 cm^{-1} is attributed to the ν_3 antisymmetric stretching vibration of the uranyl ion, UO_2^{2+}. A very strong band at 834 cm^{-1} is assigned the ν_1 symmetric U–O stretching vibration of UO_2^{2+}. The inferred

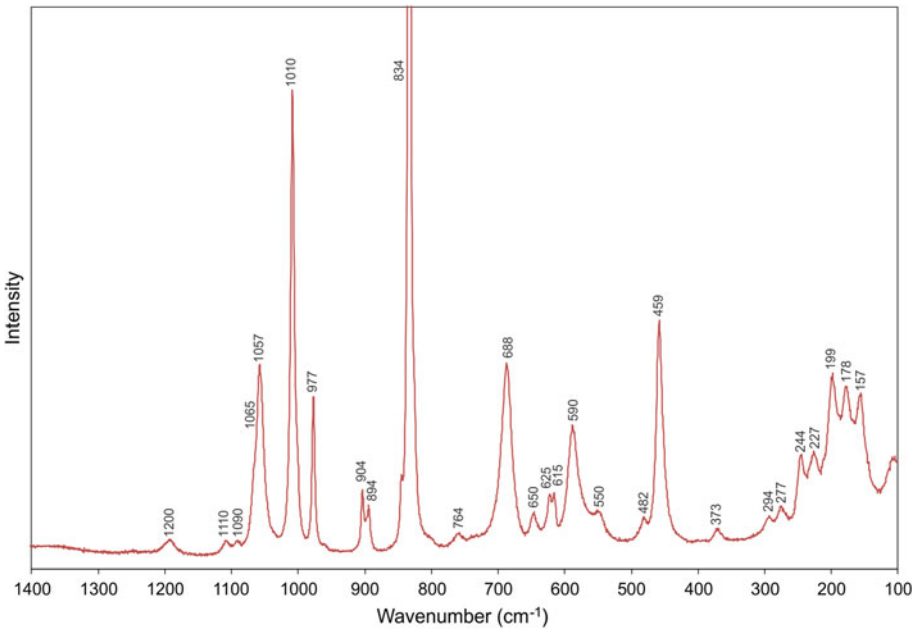

Fig. 4. Raman spectrum of ammoniomathesiusite recorded using a 785 nm diode laser.

Table 1. Chemical composition (in wt.%) for ammoniomathesiusite.

Constituent	Mean	Range	S.D.	Standard	Normalised
$(NH_4)_2O$	7.35	6.38–7.89	0.57	syn. Cr_2N	7.06
V_2O_5	5.38	5.02–5.84	0.30	V metal	5.17
UO_3	67.95	67.40–69.04	0.60	syn. UO_2	65.26
SO_3	19.02	19.02–20.07	0.40	baryte	18.27
H_2O*	4.42				4.25
Total	104.12				100.01

* Based on structure with O = 33; S.D. – standard deviation.

Table 2. Powder X-ray data (*d* in Å) for ammoniomathesiusite. Only calculated lines with $I \geq 2$ are included.

I_{obs}	d_{obs}	d_{calc}	I_{calc}	*hkl*
46	10.57	10.5645	53	110
		7.4703	3	200
62	7.10	7.1020	60	001
100	6.41	6.4142	100	101
4	5.91	5.8940	5	111
11	5.28	5.2823	14	220
5	5.13	5.1471	4	201
7	4.85	4.8664	6	211
27	4.71	4.7246	33	310
12	4.244	4.2385	12	221
4	4.093	4.0775	2	301
22	3.933	3.9337	25	311
25	3.575	3.5791	27	321
		3.5215	4	330
26	3.460	3.4548	25	102
35	3.340	3.3408	38	240
44	3.226	3.2277	50	141
25	3.140	3.1550, 3.1357	11, 15	331, 212
3	3.024	3.0230	28	241
15	2.926	2.9301	18	150
		2.8913	3	302
		2.7542	2	341
24	2.703	2.7086, 2.6964	14, 16	151, 322
12	2.578	2.5842, 2.5623	11, 10	251, 530
21	2.539	2.5362	22	412
		2.3673	2	003
7	2.359	2.3623	8	620
2	2.294	2.2863	3	342
4	2.232	2.2416, 2.2314	3, 2	621, 213
		2.2167	2	541
11	2.184	2.1862	13	252
4	2.153	2.1603	6	223
22	2.119	2.1251, 2.1165, 2.1129	14, 8, 6	631, 313, 170
13	2.0687	2.0719, 2.0555	11, 4	460, 323
7	2.0358	2.0440, 2.0252	4, 4	701, 171
9	1.9886	1.9890, 1.9819	7, 6	461, 143
		1.9716	2	721
10	1.9666	1.9618	6	730
		1.9500	3	452
14	1.9337	1.9315	14	423
15	1.8855	1.8910, 1.8868	4, 14	731, 632
8	1.8530	1.8676, 1.8471 , 1.8414	6, 5,4	800, 561, 153
7	1.8313	1.8293	5	702
12	1.8000	1.8062, 1.8008, 1.7931	7,3,9	801, 253, 181
6	1.7803	1.7755	4	004
2	1.7395	1.7388, 1.7368	2, 3	533, 570
		1.6979	2	381
14	1.6846	1.6871, 1.6841, 1.6830	3, 10, 3	571, 562, 224
		1.6722	3	623
7	1.6636	1.6620	6	314
12	1.6407	1.6429	14	182
		1.6221	2	633
		1.5852	2	703
		1.5799	2	291
		1.5764	2	553
		1.5749	3	390
16	1.5698	1.5688, 1.5678, 1.5591	2, 10, 4	382, 244, 463
		1.5375	3	391
4	1.5155	1.5185, 1.5105	5, 2	154, 733
		1.5038	2	902
		1.4879	2	563
4	1.4816	1.4835	4	491
9	1.4609	1.4662, 1.4650, 1.4594	5, 2, 5	803, 1020, 534

U–O bond lengths (after Bartlett and Cooney, 1989) for the uranyl ion of ~1.78 Å (from ν_1), 1.79 Å (from ν_3; 894) and 1.78 Å (from ν_3; 904) are in line with those derived from our X-ray structure study (see below). A very weak band at 764 cm^{-1} can be attributed to the libration mode of the H_2O or to the stretching V–O_{eq} vibration. A broader band at 688 cm^{-1}, along with the weak band at 650 cm^{-1}, can be related to V–O_{eq} vibrations (*cf.* Plášil *et al.*, 2014; Knyazev, 2000; Chernorukov *et al.*, 2000). The two-component band with maxima at 625 and 615 cm^{-1} is attributed to the ν_4 (δ) triply degenerated antisymmetric stretching vibrations of the SO_4 tetrahedron. Broad bands at 590 and 550 cm^{-1} are probably related to the V–O_{eq} vibrations as well. Raman bands at 482 and at 459 cm^{-1} are related to the split ν_2 (δ) doubly degenerate bending vibrations of the SO_4 tetrahedron. A very weak band at 373 cm^{-1} is related to the $\nu_{Rotational}$ of NH_4^+ (Heyns *et al.*, 1987). The split ν_2 (δ) UO_2^{2+} doubly degenerate bending vibrations are represented by the broader component band at 244 cm^{-1}. The rest of the bands are related to the unclassified lattice modes.

Chemical composition

Chemical analyses (seven points on six crystals) were performed at the University of Utah, USA on a Cameca SX-50 electron microprobe with four wavelength dispersive spectrometers and using *Probe for EPMA* software. Analytical conditions were 15 kV accelerating voltage, 10 nA beam current and a beam diameter of 5 μm. Counting times were 30 s on peak and 30 s on background for each element. Raw X-ray intensities were corrected for matrix effects with a φρ(z) algorithm (Pouchou and Pichoir, 1991). Time-dependent intensity corrections were applied to N, U, V and S. Wave-scans across Mg, Al, Na and K peak positions showed these elements to be absent.

Because insufficient material is available for a direct determination of H_2O, it is calculated based upon the structure determination. The crystals did not take a good polish and there was minor beam damage. The loss of weakly held H_2O under vacuum and/or during analyses would account for the high electron microprobe analytical totals when calculated H_2O is included. The somewhat lower analysed $(NH_4)_2O$ content compared to that indicated by the structure refinement (4.75 *vs.* 4.92 N atoms per formula unit) could be due to a small amount of H_3O^+ in place of NH_4^+ in the structure; however, the presence of H_3O^+ would imply highly acidic conditions. Considering that H_3O^+ has not been confirmed in any other phases in the Burro mine mineral assemblages, it seems more likely that the somewhat low analysed $(NH_4)_2O$ content

Table 3. Data collection and structure refinement details for ammoniomathesiusite.

Crystal data	
Structural formula	$(NH_4)_{4.92}(UO_2)_4(SO_4)_4(VO_5)\cdot 4H_2O$
Crystal size (μm)	140 × 70 × 35
Space group	*P*4/*n*
Unit-cell dimensions (Å)	*a* = 14.9405(9), *c* = 7.1020(5)
V (Å^3)	1585.30(18)
Z	2
Density (for above formula) (g cm^{-3})	3.680
Data collection	
Diffractometer	Rigaku R-Axis Rapid II
X-ray radiation/power	Mo*K*α (λ = 0.71075 Å)/50 kV, 40 mA
Temperature (K)	293(2)
Absorption coefficient (mm^{-1})	21.033
F(000)	1562.9
θ range (°)	3.46 to 27.49
Index ranges	$-19 \le h \le 19$, $-19 \le k \le 19$, $-8 \le l \le 9$
Reflections collected/unique	10,871/1815; R_{int} = 0.039
Reflections with $I > 2\sigma I$	1602
Completeness to θ = 27.49°	99.5%
Refinement	
Refinement method	Full-matrix least-squares on F^2
Parameter/restraints	130/20
GoF	1.077
Final *R* indices [$I > 2\sigma I$]	R_1 = 0.0218, wR_2 = 0.0443
R indices (all data)	R_1 = 0.0271, wR_2 = 0.0459
Largest diff. peak/hole (e^- Å^{-3})	+1.38/–0.73

$R_{int} = \Sigma|F_o^2-F_o^2(\text{mean})|/\Sigma[F_o^2]$. GoF = $S = \{\Sigma[w(F_o^2-F_c^2)^2]/(n-p)\}^{1/2}$. $R_1 = \Sigma||F_o|-|F_c||/\Sigma|F_o|$. $wR_2 = \{\Sigma[w(F_o^2-F_c^2)^2]/\Sigma[w(F_o^2)^2]\}^{1/2}$; $w = 1/[\sigma^2(F_o^2)+(aP)^2+bP]$ where *a* is 0.0147, *b* is 5.5409 and *P* is $[2F_c^2+\text{Max}(F_o^2,0)]/3$.

Table 4. Atom coordinates and displacement parameters (Å^2) for ammoniomathesiusite.

	x/a	*y/b*	*z/c*	U_{eq}	U^{11}	U^{22}	U^{33}	U^{23}	U^{13}	U^{12}
N1	0.1123(3)	0.2997(4)	0.3761(6)	0.0337(11)	0.031(3)	0.046(3)	0.024(2)	−0.003(2)	0.000(2)	−0.003(2)
H1a	0.078(3)	0.250(2)	0.359(7)	0.050						
H1b	0.096(3)	0.337(3)	0.284(6)	0.050						
H1c	0.1674(19)	0.282(3)	0.364(7)	0.050						
H1d	0.100(3)	0.323(3)	0.485(4)	0.050						
N2*	0	0	0	0.051(5)	0.029(5)	0.029(5)	0.094(12)	0	0	0
H2	−0.009(5)	0.0475(11)	0.0726(18)	0.050						
U	0.30770(2)	0.06726(2)	0.13503(2)	0.01279(7)	0.01107(10)	0.01043(10)	0.01685(10)	−0.00077(6)	−0.00005(6)	0.00021(6)
S	0.80289(7)	0.14358(7)	0.12364(16)	0.0150(2)	0.0117(5)	0.0109(5)	0.0225(6)	0.0006(4)	0.0005(4)	−0.0010(4)
V	0.5	0	0.3274(2)	0.0107(3)	0.0092(4)	0.0092(4)	0.0136(7)	0	0	0
O1	0.8082(2)	0.0460(2)	0.1593(5)	0.0221(8)	0.0178(17)	0.0122(16)	0.036(2)	0.0038(15)	−0.0007(15)	−0.0020(14)
O2	0.3411(2)	0.0371(2)	−0.0977(5)	0.0222(7)	0.0238(18)	0.0193(17)	0.0235(18)	−0.0037(14)	0.0005(15)	0.0016(15)
OW3	0.0000(4)	0.1354(4)	0.3922(8)	0.0621(15)	0.054(3)	0.060(4)	0.072(4)	−0.012(3)	−0.016(3)	0.006(3)
H3a	0.005(5)	0.093(3)	0.327(7)	0.050						
H3b	0.023(5)	0.129(4)	0.491(5)	0.050						
O4	0.2696(2)	0.0993(2)	0.3626(4)	0.0219(7)	0.0214(18)	0.0236(18)	0.0207(17)	−0.0053(14)	0.0046(14)	−0.0028(15)
O5	0.8746(2)	0.1663(2)	−0.0104(5)	0.0226(8)	0.0137(16)	0.0153(17)	0.039(2)	0.0040(15)	0.0083(15)	0.0015(14)
O6	0.7157(2)	0.1615(2)	0.0306(5)	0.0186(7)	0.0129(15)	0.0176(17)	0.0254(17)	0.0055(14)	0.0009(14)	0.0010(14)
O7	0.3910(2)	−0.0504(2)	0.2496(4)	0.0155(7)	0.0128(15)	0.0116(15)	0.0220(17)	−0.0029(13)	−0.0013(13)	0.0007(13)
O8	0.8118(3)	0.1925(2)	0.2979(5)	0.0289(8)	0.033(2)	0.025(2)	0.0282(19)	−0.0061(16)	−0.0057(17)	0.0006(17)
O9	0.5	0	0.5521(10)	0.0304(17)	0.034(3)	0.034(3)	0.023(4)	0	0	0

* N2 site refined occupancy = 0.92(4).

Table 5. Selected bond distances (Å) for ammoniomathesiusite.

U–O4	1.779(3)	N1–O4	2.973(6)	N2–O5 (× 4)	3.113(3)	S–O8	1.443(4)
U–O2	1.785(3)	N1–O8	2.975(6)	N2–O1 (× 4)	3.156(3)	S–O5	1.473(3)
U–O7	2.302(3)	N1–OW3	2.975(8)	N2–OW3 (× 4)	3.442(6)	S–O1	1.483(3)
U–O7	2.355(3)	N1–O6	2.989(5)	<N2–O>	3.237	S–O6	1.486(3)
U–O6	2.383(3)	N1–O2	3.046(6)			<S–O>	1.471
U–O1	2.427(3)	N1–O8	3.093(6)	V–O9	1.596(7)		
U–O5	2.449(3)	N1–O7	3.128(5)	V–O7 (× 4)	1.876(3)	Hydrogen Bonds*	
<U–O_{Ur}>	1.782	N1–O2	3.216(6)	<V–O>	1.820	OW3–O4	3.041(7)
<U–O_{eq}>	2.383	N1–O9	3.469(5)			OW3–O8	3.013(7)
		<N1–O>	3.096				

* Note that there are no obvious hydrogen bonds through H3a and there are two apparent hydrogen bonds through H3b.

Table 6. Bond-valence analysis for ammoniomathesiusite. Values are expressed in valence units.*

	U	S	V	N1	N2	H bonds	Σ
O1	0.45	1.46			0.08 $^{\times 4\downarrow}$		1.99
O2	1.74			0.11, 0.07			1.92
OW3				0.13	0.04 $^{\times 4\downarrow}$	−0.12	0.09
O4	1.76			0.13		0.06	1.95
O5	0.43	1.50			0.09 $^{\times 4\downarrow}$		2.02
O6	0.49	1.45		0.13			2.07
O7	0.58, 0.52		0.82 $^{\times 4\downarrow}$	0.09			2.01
O8		1.61		0.13, 0.10		0.06	1.90
O9			1.69	0.03 $^{\times 4\rightarrow}$			1.81
Σ	5.96	6.02	4.97	0.92	0.84		

* NH_4^+–O bond valence parameters from Garcia-Rodriguez *et al.* (2000). U^{6+}–O, V^{5+}–O and S^{6+}–O bond-valence parameters are from Gagné and Hawthorne (2015). Hydrogen-bond strengths associated with OW3 are based on O–O bond lengths from Ferraris and Ivaldi (1988).

Table 7. Comparison of ideal formulas, cell parameters, optical properties and calculated densities (ideal) for ammoniomathesiusite and mathesiusite (Plášil *et al.*, 2014).

	Ammoniomathesiusite	Mathesiusite
Ideal formula	$(NH_4)_5(UO_2)_4(SO_4)_4(VO_5)\cdot 4H_2O$	$K_5(UO_2)_4(SO_4)_4(VO_5)\cdot 4H_2O$
Space group	*P*4/*n*	*P*4/*n*
a (Å)	14.9405(9)	14.9704(10)
c (Å)	7.1020(5)	6.8170(5)
V (Å^3)	1585.30(18)	1527.78(18)
Z	2	2
Optical class	Uniaxial (–)	Uniaxial (–)
ω	1.653(2)	1.634(3)
ϵ	1.609(2)	1.597(3)
Pleochroism	*O* = green yellow, *E* = colourless	None observed (colourless)
Density (g cm^{-3})	3.681	4.049

is due to loss under vacuum (along with the H_2O noted above) prior to analyses. The results are given in Table 1.

The empirical formula (calculated on the basis of 33 O atoms per formula unit) is $[(NH_4)_{4.75}(U_{1.00}O_2)_4(S_{1.00}O_4)_4(V_{1.00}O_5)\cdot 4(H_{2.07}O)$ [Excess H is included for charge balance]. The ideal formula is $(NH_4)_5(UO_2)_4(SO_4)_4(VO_5)\cdot 4H_2O$, which requires $(NH_4)_2O$ 7.41, V_2O_5 5.17, UO_3 65.10, SO_3 18.22 and H_2O 4.10, total 100.00 wt.%. The Gladstone-Dale compatibility index $1 - (K_P/K_C)$ for the empirical formula is 0.009, in the superior range (Mandarino, 2007), using $k(UO_3) = 0.118$, as provided by Mandarino (1976).

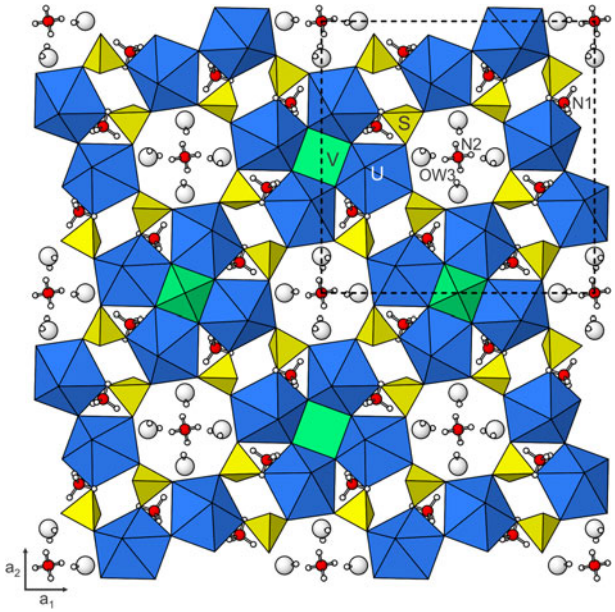

Fig. 5. The structure of ammoniomathesiusite viewed down **c**. The unit-cell outline is shown by dashed lines.

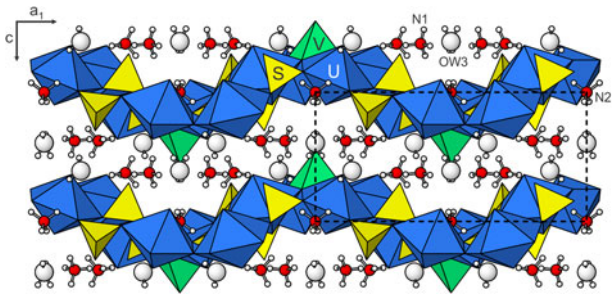

Fig. 6. The structure of ammoniomathesiusite viewed down $\mathbf{a_2}$. The unit-cell outline is shown by dashed lines.

X-ray crystallography and structure refinement

Powder X-ray studies were done using a Rigaku R-Axis Rapid II curved imaging plate microdiffractometer, with monochromatised Mo*K*α radiation (λ = 0.71075 Å). A Gandolfi-like motion on the ϕ and ω axes was used to randomise the samples. Observed *d* values and intensities were derived by profile fitting using *JADE 2010* software (Materials Data, Inc.). The powder data presented in

Table 2 show good agreement with the pattern calculated from the structure determination. Unit-cell parameters refined from the powder data using *JADE 2010* with whole pattern fitting are a = 14.9519(14), c = 7.1083(8) Å and V = 1589.1(3) Å^3.

The single-crystal structure data were collected at room temperature using the same diffractometer and radiation noted above. The data were processed using the Rigaku *CrystalClear* software package and an empirical (multi-scan) absorption correction was applied using the *ABSCOR* program (Higashi, 2001) in the *CrystalClear* software suite. The structure was solved by direct methods using *SIR2011* (Burla *et al.*, 2012). *SHELXL-2016* (Sheldrick, 2015) was used for the refinement of the structure.

Difference-Fourier syntheses located all non-hydrogen atoms not located in the original structure solution, and subsequent cycles located all H sites. The structure was found to be identical to that of mathesiusite (Plášil *et al.*, 2014) and all atom sites were transformed to correspond to that structure, with two NH_4 sites in place of the two K sites in mathesiusite. The H atom sites associated with OW3 were refined with soft restraints of 0.82(3) Å on the O–H distances and 1.30(3) Å on the H–H distances, and those for the H sites associated with N1 and N2, with soft restraints of 0.90(3) Å on the O–H distances and 1.45(3) Å on the H–H distances. The U_{eq} of each H was set to 0.05. All non-hydrogen sites refined to full occupancy, except the N2 site, which refined to an occupancy of 0.92(4). Data collection and refinement details are given in Table 3, atom coordinates and displacement parameters in Table 4, selected bond distances in Table 5 and a bond-valence analysis in Table 6. A comparison of the ideal formulas, cell parameters, optical properties and calculated densities (ideal) for ammoniomathesiusite and mathesiusite is provided in Table 7.

The crystallographic information files have been deposited with the Principal Editor of *Mineralogical Magazine* and are available as Supplementary material (see below).

Description and discussion of the structure

The U site in the structure of ammoniomathesiusite is surrounded by seven O atoms forming a squat UO_7 pentagonal bipyramid. This is the most typical coordination for U^{6+}, particularly in uranyl sulfates, where the two short apical bonds of the bipyramid constitute the UO_2 uranyl group (Burns, 2005). Sulfur is coordinated by four O atoms at the distances typical for tetrahedral coordination, ~1.47 Å. Vanadium is in square pyramidal coordination, bonded strongly to one O atom at the distance of 1.596 Å (vanadyl bond; *cf.* Schindler *et al.*, 2000) and four O atoms at the distances of 1.876 Å. This (4 + 1) coordination is one of the characteristic environments for the V^{5+} cation (Schindler *et al.*, 2000). The N1 atom ($NH_4$1 group) is [9]-coordinated with an average bond length ~3.10 Å, while the N2 atom ($NH_4$2 group) is [12]-coordinated with an average N–O bond length of ~3.24 Å (Table 5). Both NH_4 groups are linked to the only H_2O molecule (OW3) in the structure.

The structure (Figs 5 and 6) contains heteropolyhedral sheets based on $[(UO_2)_4(SO_4)_4(VO_5)]^{5-}$ clusters. These clusters arise from linkages between corner-sharing quartets of uranyl pentagonal bipyramids, which define a square-shaped void at the centre of which is the base of the VO_5 square pyramid. Adjacent corner-shared uranyl pentagonal bipyramids are also linked through SO_4 tetrahedra, with which they share corners. Each SO_4 shares a third vertex with a uranyl pentagonal bipyramid in another cluster to form the sheets. The NH_4^+ cations are located between the sheets, together with the H_2O group. The corrugated sheets are stacked perpendicular to **c**. These heteropolyhedral sheets are similar to those in the structures of synthetic uranyl chromates (Unruh *et al.*, 2012) and molybdates (Obbade *et al.*, 2003).

Supplementary material. To view supplementary material for this article, please visit https://doi.org/10.1180/mgm.2018.112

Acknowledgements. Structures Editor Peter Leverett and an anonymous reviewer are thanked for their constructive comments on the manuscript. A portion of this study was funded by the John Jago Trelawney Endowment to the Mineral Sciences Department of the Natural History Museum of Los Angeles County. We would like to thank Don Coram, the owner of the Burro mine, for allowing us access to the property, and to Okie Howell and Jess Fulbright for providing logistical support during our visits.

References

Bartlett J.R. and Cooney R.P. (1989) On the determination of uranium-oxygen bond lengths in dioxouranium(VI) compounds by Raman spectroscopy. *Journal of Molecular Structure*, **193**, 295–300.

Burla M.C., Caliandro R., Camalli M., Carrozzini B., Cascarano G.L., Giacovazzo C., Mallamo M., Mazzone A., Polidori G. and Spagna R. (2012) *SIR*2011: a new package for crystal structure determination and refinement. *Journal of Applied Crystallography*, **45**, 357–361.

Burns P.C. (2005) U^{6+} minerals and inorganic compounds: insights into an expanded structural hierarchy of crystal structures. *The Canadian Mineralogist*, **43**, 1839–1894.

Carter W.D. and Gualtieri J.L. (1965) Geology and uranium–vanadium deposits of the La Sal quadrangle, San Juan County, Utah, and Montrose County, Colorado. *United States Geological Survey Professional Paper*, **508**.

Chernorukov N.G., Suleymanov E.V., Knyazev A.V., Vyshinski N.N. and Klimov E.Y. (2000) Vibrational spectra of uranyl vanadates of mono- and divalent metals. *Zhurnal Obshchey Khimii*, **70**, 1418–1424.

Evans Jr. H.T. (1991) Metamunirite, a new anhydrous sodium metavanadate from San Miguel County, Colorado. *Mineralogical Magazine*, **55**, 509–513.

Ferraris G. and Ivaldi G. (1988) Bond valence vs. bond length in O···O hydrogen bonds. *Acta Crystallographica*, **B44**, 341–344.

Friedel C. and Cumenge E. (1899) Sur un nouveau minerai d'urane, la carnotite. *Comptes rendus de l'Académie des sciences de Paris*, **128**, 532–534.

Frost R.L., Erickson K.L., Weier M.L. and Carmody O. (2005) Raman and infrared spectroscopy of selected vanadates. *Spectrochimica Acta, Part A: Molecular and Biomolecular Spectroscopy*, **61A**, 829–834.

Gagné O.C. and Hawthorne F.C (2015) Comprehensive derivation of bond-valence parameters for ion pairs involving oxygen. *Acta Crystallographica*, **B71**, 562–578.

García-Rodríguez L., Rute-Pérez Á., Piñero J.R. and González-Silgo C. (2000) Bond-valence parameters for ammonium-anion interactions. *Acta Crystallographica*, **B56**, 565–569.

Heyns A.M., Venter M.W. and Range K.-J. (1987) The vibrational spectra of NH_4VO_3 at elevated temperatures and pressures. *Zeitschrift für Naturforshung*, **42b**, 843–852.

Higashi T. (2001) *ABSCOR*. Rigaku Corporation, Tokyo.

Kampf A.R., Nash B.P., Marty J. and Hughes J.M. (2017) Burroite, $Ca_2(NH_4)_2(V_{10}O_{28})\cdot 15H_2O$, a new decavanadate mineral from the Burro mine, San Miguel County, Colorado. *The Canadian Mineralogist*, **55**, 473–481.

Kampf A.R., Plášil J., Olds T.A., Nash B.P. and Marty J. (2018) Ammoniozippeite, a new uranyl sulfate from the Blue Lizard mine, San Juan County, Utah, and the Burro mine, San Miguel County, Colorado, USA. *The Canadian Mineralogist*, **56**, 235–245.

Knyazev A.V. (2000) *Synthesis, structure and properties of uranyl vanadates of mono-, di- and trivalent metals*. PhD thesis, N.I. Lobachevsky State University of Nizhny Novgorod, Russia.

Mandarino J.A. (1976) The Gladstone-Dale relationship – Part 1: derivation of new constants. *The Canadian Mineralogist*, **14**, 498–502.

Mandarino J.A. (2007) The Gladstone–Dale compatibility of minerals and its use in selecting mineral species for further study. *The Canadian Mineralogist*, **45**, 1307–1324.

Obbade S., Yagoubi S., Dion C., Saadi. M. and Abraham F. (2003) Synthesis, crystal structure and electrical characterization of two new potassium uranyl molybdates $K_2(UO_2)_2(MoO_4)O_2$ and $K_8(UO_2)_8(MoO_5)_3O_6$. *Journal of Solid State Chemistry*, **174**, 19–31.

Plášil J., Veselovský F., Škoda R., Novák M., Sejkora J., Čejka J., Škácha P. and Kasatkin A.V. (2014) Mathesiusite, $K_5(UO_2)_4(SO_4)_4(VO_5)(H_2O)_4$, a new uranyl vanadate-sulfate from Jáchymov, Czech Republic. *American Mineralogist*, **99**, 625–632.

Pouchou J.L. and Pichoir F. (1991) Quantitative analysis of homogeneous or stratified microvolumes applying the model "PAP". Pp. 31–75 in: *Electron Probe Quantification* (K.F.J. Heinrich and D.E. Newbury, editors). Plenum Press, New York.

Schindler M., Hawthorne F.C. and Baur W.H. (2000) Crystal chemical aspects of vanadium: polyhedral geometries, characteristic bond valences, and polymerization of (VO_n) polyhedra. *Chemistry of Materials*, **12**, 1248–1259

Shawe D.R. (2011) Uranium-vanadium deposits of the Slick Rock district, Colorado. *United States Geological Survey Professional Paper*, **576-F**.

Sheldrick G.M. (2015) Crystal Structure refinement with *SHELX*. *Acta Crystallographica*, **C71**, 3–8.

Unruh D.K., Quicksall A., Pressprich L., Stoffer M., Qiu J., Nuzhdin K., Wub W., Vyushkova M. and Burns P.C. (2012) Synthesis, characterization, and crystal structures of uranyl compounds containing mixed chromium oxidation states. *Journal of the Solid State Chemistry*, **191**, 162–166.